

Signal and background considerations for the MRSt on the National Ignition Facility (NIF)

C. W. Wink, J. A. Frenje, T. J. Hillsabeck, R. Bionta, H. Y. Khater, M. Gatu Johnson, J. D. Kilkenny, C. K. Li, F. H. Séguin, and R. D. Petrasso

Citation: [Review of Scientific Instruments](#) **87**, 11D808 (2016); doi: 10.1063/1.4958938

View online: <http://dx.doi.org/10.1063/1.4958938>

View Table of Contents: <http://scitation.aip.org/content/aip/journal/rsi/87/11?ver=pdfcov>

Published by the [AIP Publishing](#)

Articles you may be interested in

[Development of a polar direct-drive platform for studying inertial confinement fusion implosion mix on the National Ignition Facility](#))

Phys. Plasmas **20**, 056310 (2013); 10.1063/1.4803886

[Detailed implosion modeling of deuterium-tritium layered experiments on the National Ignition Facility](#))

Phys. Plasmas **20**, 056318 (2013); 10.1063/1.4802194

[Stimulated Raman scatter analyses of experiments conducted at the National Ignition Facility](#) a)

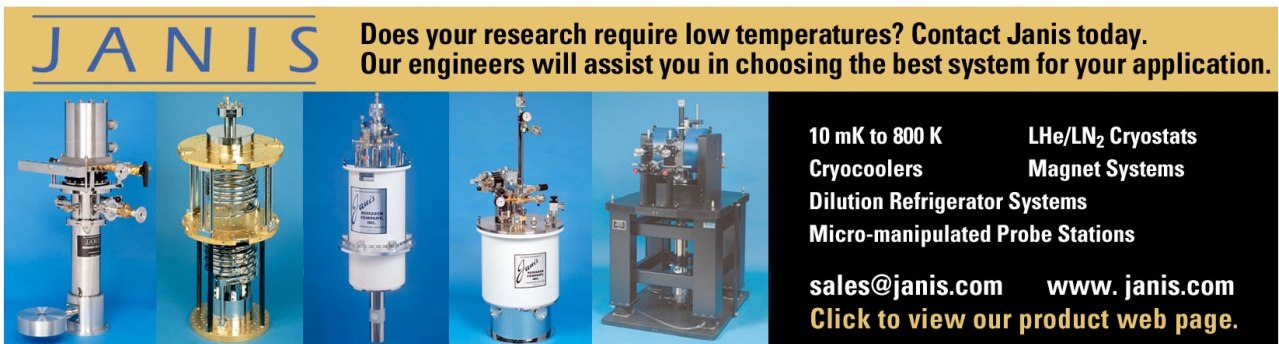
Phys. Plasmas **18**, 056312 (2011); 10.1063/1.3577836

[Analysis of the National Ignition Facility ignition hohlraum energetics experiments](#) a)


Phys. Plasmas **18**, 056302 (2011); 10.1063/1.3562552

[Reaction-in-flight neutrons as a signature for shell mixing in National Ignition Facility capsules](#)

Phys. Plasmas **17**, 012705 (2010); 10.1063/1.3274947



JANIS Does your research require low temperatures? Contact Janis today.
Our engineers will assist you in choosing the best system for your application.



10 mK to 800 K LHe/LN₂ Cryostats
Cryocoolers Magnet Systems
Dilution Refrigerator Systems
Micro-manipulated Probe Stations

sales@janis.com www.janis.com
Click to view our product web page.

Signal and background considerations for the MRSt on the National Ignition Facility (NIF)

C. W. Wink,^{1,a)} J. A. Frenje,¹ T. J. Hillsabeck,² R. Bionta,³ H. Y. Khater,³ M. Gatu Johnson,¹ J. D. Kilkenny,² C. K. Li,¹ F. H. Séguin,¹ and R. D. Petrasso¹

¹Massachusetts Institute of Technology, Cambridge, Massachusetts 02139, USA

²General Atomics, San Diego, California 92186, USA

³Lawrence Livermore National Laboratory, Livermore, California 94550, USA

(Presented 7 June 2016; received 7 June 2016; accepted 22 June 2016; published online 3 August 2016)

A Magnetic Recoil Spectrometer (MRSt) has been conceptually designed for time-resolved measurements of the neutron spectrum at the National Ignition Facility. Using the MRSt, the goals are to measure the time-evolution of the spectrum with a time resolution of ~ 20 -ps and absolute accuracy better than 5%. To meet these goals, a detailed understanding and optimization of the signal and background characteristics are required. Through ion-optics, MCNP simulations, and detector-response calculations, it is demonstrated that the goals and a signal-to background >5 –10 for the down-scattered neutron measurement are met if the background, consisting of ambient neutrons and gammas, at the MRSt is reduced 50–100 times. *Published by AIP Publishing.* [<http://dx.doi.org/10.1063/1.4958938>]

I. INTRODUCTION

The current suite of neutron diagnostics on the National Ignition Facility (NIF)¹ has been used extensively for measurements of the time-integrated neutron spectrum, from which burn-averaged values of areal density (ρR), yield (Y_n), and apparent ion temperature (T_i) in an Inertial Confinement Fusion (ICF) have been determined.^{2–9} Although these diagnostics have been essential for guiding the ignition experiments toward the regime of burning plasmas, it has become clear that new, transformational neutron diagnostics are required to provide detailed information about the time evolution of the fuel assembly, hot core ion temperature, nuclear burn, and alpha-particle heating. As discussed by Frenje *et al.*,¹⁰ this information can be obtained simultaneously with the next-generation magnetic recoil spectrometer (MRS), called MRSt for time-resolved measurements of the ICF neutron spectrum. For successful implementation of the MRSt on the NIF, a detailed understanding and optimization of the signal and background are required, where the latter is mainly due to unscattered neutrons and scattered neutrons and gammas from nearby structures. Through ion-optics, MCNP simulations, and detector-response calculations, an assessment of the signal and background at an unshielded MRSt has been made to determine the required reduction of background to meet the goal of measuring the neutron spectrum with a time resolution of ~ 20 -ps and absolute accuracy better than 5%.

This paper is structured as follows: Section II briefly discusses the MRSt design. Section III elaborates on the Cesium-Iodide (CsI)-photocathode response to ions, gammas,

and neutrons. Section IV discusses the signal and background levels for an unshielded MRSt and their implications in terms of required shielding surrounding the MRSt. Section V discusses the path forward.

II. MRSt DESIGN

The MRSt design consists of a small CH₂ (or CD₂) foil positioned very close to the implosion for minimization of the time spread of different-energy neutrons that produce recoil protons (or deuterons) with the same energy; an aperture positioned 600 cm from the foil for selection of forward-scattered recoil protons (or deuterons); two magnets (with opposing B-field directions) located just outside the NIF target chamber, for energy dispersion and focusing of the recoil protons (or deuterons) without introducing any significant time spread; and a pulse-dilation drift tube with a CsI photocathode¹¹ for detection of the recoil protons (or deuterons) over an energy range of 12–16 MeV (or 10.7–14.2 MeV). The CsI photocathode will be about 20 cm long covering the complete energy range and about 2 cm in the direction perpendicular to the dispersive plane. The signal protons (or deuterons) arrive at the focal plane of the spectrometer, where the CsI photocathode is positioned, during the time interval of 159–187 ns (or 238–279 ns). To record the signal with 20-ps time resolution and with a limited set of energy channels at the backend of the pulse-dilation drift tube, the signal distribution will be deskewed and stretched by the pulse-dilation drift tube, as discussed briefly in the next paragraph and in detail by Hillsabeck *et al.*¹¹

For the MRSt pulse-dilation drift tube, the plan is to use a 1000-Å-thick CsI photocathode, which produces secondary electrons (SE) in response to energy deposited by signal protons (or deuterons), and background neutrons and γ -rays. The secondary electrons emitted from the backside of the

Note: Contributed paper, published as part of the Proceedings of the 21st Topical Conference on High-Temperature Plasma Diagnostics, Madison, Wisconsin, USA, June 2016.

^{a)}Author to whom correspondence should be addressed. Electronic mail: cwink@mit.edu.

CsI photocathode are accelerated by a spatially varying and time-varying electric field that deskews and stretches the secondary-electron distribution, while it drifts about ~ 1 m. To effectively collect the emitted secondary electrons, a magnetic field parallel to the symmetry axis of the tube confines the electrons. A microchannel plate (MCP) at the backend of the pulse-dilation drift tube provides gain before the signal is detected by an array of segmented anodes (along the energy axis) connected to a multi-channel digitizer. From the time-resolved histogram of secondary electrons, the time-resolved spectrum of the emitted neutrons will be determined.

III. CsI RESPONSE TO IONS, γ -RAYS, AND NEUTRONS

Protons (or deuterons) interacting with the CsI photocathode deposit part of their energy and generate a cascade of primary electrons. As the CsI cathode is thin, a very small fraction of the primary-electron energy is deposited, and about half of this energy goes to exciting the atoms and the other half goes to ionizing the atoms, generating free secondary electrons. The generation of a secondary electron requires a minimum energy deposited, which is material dependent. For CsI, this has been determined to be ~ 20 eV¹² or ~ 70 eV.¹³ A fraction of the generated secondary electrons are emitted from the back side of the CsI photocathode, which can be modeled by $P_0 \exp(-\frac{x}{L})$, where P_0 is the probability for a secondary-electron to escape if generated at $x = 0$ ($\sim 70\%$ for CsI), L is the escape length (~ 90 Å for CsI), and x is the distance between the birth location and the back side of the CsI photocathode.¹² As the proton (or deuteron) energy deposition scales roughly linearly with CsI thickness, the number of secondary-electrons (SE) emitted on the back side of the CsI photocathode can be expressed as $\int (dE/dx) P_0 \exp(-\frac{x}{L}) dx$ from zero to x .

For example, the stopping power of a 14-MeV proton is ~ 0.8 eV/Å in CsI, which means that it deposits 800 eV when traversing the 1000-Å-thick CsI photocathode. Half of this energy ionizes the atom and generates secondary electrons. Using ~ 40 eV as the average energy required to generate a secondary electron in CsI, ~ 10 secondary electrons are produced while ~ 0.7 escape the backside of the CsI photocathode. In the case of a 12.4-MeV deuteron, the stopping power is 1.3 eV/Å and ~ 18 secondary electrons are produced while 1.1 escape. These numbers agree well with the Henke model,¹⁴ experimentally tested by Kravchenko *et al.*,¹⁵ even though their model uses a secondary-electron-escape depth of 250 μm and 250 eV as the minimum energy required to generate one secondary electron in the CsI material.

Regarding the background, neutrons interact with the CsI photocathode through elastic and inelastic processes, primarily generating charged particles, which ionize the atoms and produce secondary electrons in a similar fashion as described above. Thus, it is clear that the effect of the background from the CsI needs to be characterized and possibly suppressed. For example, as discussed in Sec. IV, the most probable energy of the background neutrons at the CsI is ~ 7 MeV, and the probability for this neutron to interact with the CsI photocathode is $\sim 10^{-6}$. Subsequently, the neutron-induced charged particles deposit on average about 500 eV in

the CsI. This means that about $\sim 10^{-5}$ secondary electrons are produced per incoming neutron, which is $\sim 10^5$ smaller than the level of secondary electrons generated by a signal proton.

Background γ -rays are generated from (n,n') and (n,γ) reactions in nearby structures. These γ -rays interact with the CsI photocathode through photoelectric effect, Compton scattering, and pair production, producing primary electrons and positrons, which in turn produce secondary electrons. The most probable energy of the background γ -rays at the MRSt CsI is ~ 3 MeV (see Sec. IV), and the probability for this γ -ray to interact with the CsI photocathode is $\sim 10^{-6}$. The generated primary electrons and positrons deposit on average ~ 60 eV in the CsI. This means that about 10^{-6} are produced per incoming γ -ray, which is about 10^6 smaller than the level of secondary electrons generated by a signal proton. The level of secondary electrons generated by a proton (or deuteron), γ -ray, and neutron provides some guidance about the CsI response to the signal and background, but does not provide detailed information about the signal-to-background (S/B). For this, an understanding of the absolute level of γ -ray and neutron flux at the MRSt CsI and MCP must be understood, which is elaborated upon in Sec. IV.

IV. SIGNAL AND BACKGROUND FOR AN UNSHIELDED MRSt

For successful implementation of the MRSt for time-resolved measurements of the neutron spectrum, the S/B characteristics must be optimized, which requires, first, a detailed understanding of the signal and background distributions at the CsI photocathode. Second, the CsI response to the signal and background must be understood as well. Sec. III discussed this to some extent, but a detailed experimental study of the CsI response to ions, neutrons, and γ -rays is required to obtain a fundamental understanding of the MRSt instrument response function.

The signal distribution at the CsI photocathode was calculated using detailed ion-optical simulations of the MRSt,¹⁰ and an example of the results from that modeling is shown in the top graph of Fig. 1 for protons and deuterons generated in a CH₂ and CD₂ foil, respectively (for a NIF shot producing 3.6×10^{16} n). The neutron and γ -ray's background fluxes and spectra at an unshielded MRSt CsI, but behind the NIF target chamber wall and inside the MRSt detector vacuum housing of 2.54-cm steel, were determined using a detailed MCNP model of the NIF target bay implemented by Khater and Brereton,¹⁶ and the results from that calculation are shown in the middle and bottom graphs in Fig. 1 for the same NIF shot.

The CsI response to the signal and background distributions was obtained by using a secondary-electron model discussed in Sec. III, with modifications based on the specific MRSt CsI photocathode and the relationships between ion-, neutron-, and γ -ray-induced electron energy deposition. The results from that modeling are shown in Fig. 2 where the number of secondary electrons (SEs) emitted from the backside of the CsI photocathode is plotted as function of time. As shown by the data, the background generated in the CsI is two to four orders of magnitude lower than the signal and will not significantly affect the MRSt measurement.

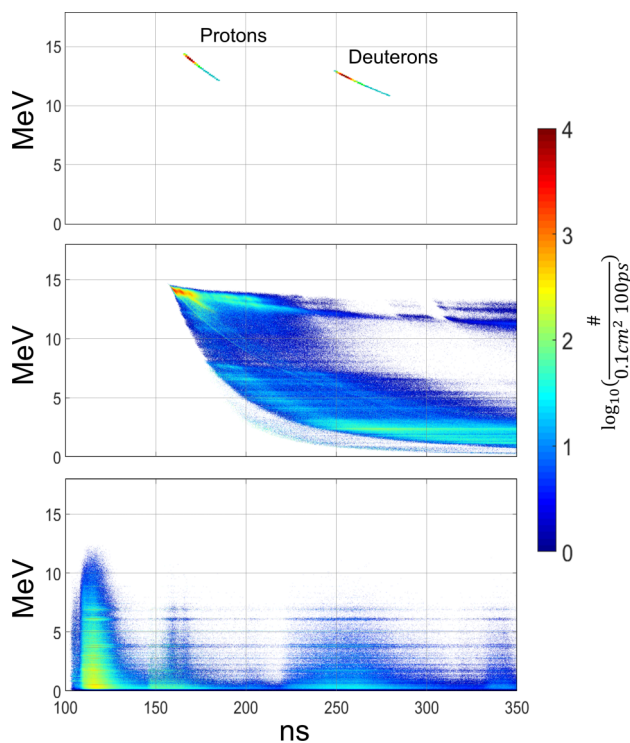


FIG. 1. Simulation of the MRSt proton and deuteron signal distributions at the CsI photocathode for a NIF shot producing 3.6×10^{16} n (top graph). For this simulation, the MRSt was configured in the low-efficiency, high-energy/temporal resolution ($\Delta E = 100$ keV and $\Delta t = 13$ ps; see Frenje *et al.*¹⁰). The protons or deuterons arrive at the CsI during the time window of 165–188 ns or 248–283 ns, respectively. The middle and bottom graph illustrate the neutron and γ -ray's background flux at the CsI photocathode, respectively. See text for more details.

The MCP on the backend of the pulse-dilation drift tube is another source of background that affects the MRSt data. Both neutrons and γ -rays interact with the MCP generating secondary electrons that will add background. The MCP sensitivity to neutrons and γ -rays is dependent on multiple factors, including the MCP open area ratio, MCP surface coating, and accelerating voltage. Medley and Persing found the detection efficiency for 2.5- and 14-MeV neutrons to be 1.7×10^{-3} and 6.4×10^{-3} secondary electrons per incoming neutron, respectively.¹⁷ For γ -rays, Timothy and Bybee found

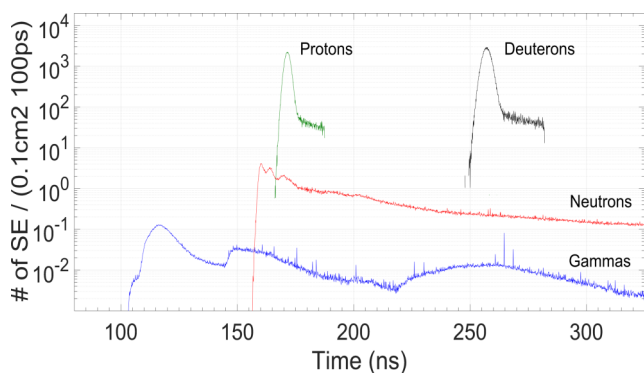


FIG. 2. Simulated number of signal- and background-generated secondary electrons emitted from the backside of the CsI photocathode for the NIF shot producing a neutron yield of 3.6×10^{16} n . See text for more details.

the detection efficiency of 1-MeV γ -rays to be $\sim 2 \times 10^{-2}$ secondary electrons per incoming photon.¹⁸ These values are for angles of perpendicular incidence at the MCP. As the background at the MCP is isotropic, and as the MCP response depends on angle and energy of the incoming neutrons and γ -rays,¹⁹ the quoted detection efficiencies represent rough estimates.

The MRSt S/B was determined by using the simulated neutron and γ -ray background fluxes at the MCP and extrapolations of the published detection efficiencies for a particular MCP. For an assessment of the required level of background reduction for successful implementation of the MRSt, the down-scattered signal was used. For protons, the down-scattered signal was determined for a single energy channel at 12.5 MeV across a 100-keV bin and 100-ps duration stretched $10 \times$ to 1 ns at the MCP. The background flux was considered for the area comparable to the size of a 100-keV bin, which is 5×20 mm². As it takes the secondary-electron ~ 50 ns to traverse the length of the pulse-dilation drift tube, the background flux at the MCP is assessed ~ 50 ns after the arrival of the down-scattered proton signal at the CsI photocathode, which corresponds to a time of 234 ns and 327 ns for the proton- and deuteron-cases, respectively.

In the case of protons, the energy integrated neutron flux at the MCP is $\sim 10^6$ n /(ns 100 mm²) and with a detection efficiency of 3×10^{-3} , the number of neutron-generated SEs in the MCP is $\sim 3 \times 10^3$ /(ns 100 mm²). For γ -rays, the flux is $\sim 6 \times 10^5$ photons/(ns 100 mm²). Given the MCP response to γ -rays with different incident angles and energies, we estimate from the work of Timothy and Bybee,¹⁸ an efficiency for detecting the dominant γ -ray (~ 3 MeV) to be $\sim 5 \times 10^{-3}$. Therefore, the number of γ -ray-generated SEs in the MCP is $\sim 3 \times 10^3$ /(ns 100 mm²). In the case of deuterons, the energy-integrated neutron flux at the MCP is $\sim 8 \times 10^5$ n /(ns 100 mm²) and with the same detection efficiency as above, the number of neutron-generated SEs in the MCP is $\sim 2 \times 10^3$ SEs/(ns 100 mm²). For γ -rays, the flux is $\sim 2 \times 10^5$ photons/(ns 100 mm²), which means that the number of γ -ray-generated SEs in the MCP is $\sim 2 \times 10^3$ SE/(ns 100 mm²). For comparison, the number of SEs from the down-scattered signal protons (or deuterons) is ~ 500 SE/(1 ns 100 mm²).

To meet the S/B requirement of 5–10 for the down-scattered neutron measurement, the background needs to be reduced about 50–100 \times . This can be achieved with either shielding, in the form of concrete or lead, or a less sensitive MCP, or a combination of the two. As there is wide variability in the MCP neutron and γ -ray detection efficiencies, an MCP will be chosen that maximizes the signal electron gain while minimizing background sensitivity.

V. CONCLUSIONS AND PATH FORWARD

Through ion-optics and MCNP simulations it is shown that the neutron and γ -ray's background generated in the CsI is two and four orders of magnitude lower in comparison to the signal, respectively, and will not significantly affect the MRSt measurement. On the other hand, the MCP poses a greater challenge from a S/B point of view. To achieve a S/B > 5 –10

for the down-scattered-signal measurement, either an MCP less sensitive to neutrons and γ -rays or substantial shielding in the form of concrete and lead surrounding the MRSt detector, or a combination of the two, must be used. It is demonstrated that the S/B goal is met if the background at MRSt is reduced 50–100 \times .

To finalize the design of the MRSt and ensure that the instrument meets the fidelity requirements, a fundamental understanding of the MRSt S/B characteristics must be obtained, as discussed in this paper. This will be accomplished by thorough tests of the CsI response to ions, neutrons, and γ -rays at the MIT Plasma Science and Fusion Center (PSFC) accelerator facility.²⁰ Currently, a DC pulse-height electron detector is being constructed at General Atomics for the experimental tests of the CsI response. Regarding the background, the MCNP model of the NIF target bay will be further refined to include a detailed and optimized shielding model of the MRSt. A Monte Carlo code for simulating the SE yield based on the method presented in McDonald *et al.*¹² is also being developed. As the characteristics of different MCPs vary significantly, care must be exercised when selecting and testing the MCP for the MRSt. The selected MCP and its response to background neutrons and γ -rays will be characterized through *in situ* testing at OMEGA (or possibly at the NIF) and MCNP simulations of the neutron and γ -ray flux at the MCP. This will provide an understanding of the MCP induced background recorded by the MRSt segmented anodes. Feasibility tests of the foil attached to the hohlraum will also be carried out at NIF. Additionally, the concomitant

deskew and pulse-dilation conditioning of the ion signal will be demonstrated.¹¹

ACKNOWLEDGMENT

This work was performed under the auspices of the U.S. Department of Energy by Lawrence Livermore National Laboratory under Contract No. DE-AC52-07NA27344.

- ¹G. H. Miller *et al.*, *Nucl. Fusion* **44**, S228 (2004).
- ²R. Hatarik *et al.*, *J. Appl. Phys.* **118**, 184502 (2015).
- ³M. Gatu Johnson *et al.*, *Rev. Sci. Instrum.* **83**, 10D308 (2012).
- ⁴T. J. Clancy *et al.*, *Proc. SPIE* **9211**, 92110A (2013).
- ⁵J. A. Frenje *et al.*, *Rev. Sci. Instrum.* **72**, 854 (2001).
- ⁶J. A. Frenje *et al.*, *Rev. Sci. Instrum.* **79**, 10E502 (2008).
- ⁷J. A. Frenje *et al.*, *Phys. Plasmas* **17**, 056311 (2010).
- ⁸D. T. Casey *et al.*, *Rev. Sci. Instrum.* **84**, 043506 (2013).
- ⁹J. A. Frenje *et al.*, *Nucl. Fusion* **53**, 043014 (2013).
- ¹⁰J. A. Frenje *et al.*, “The Magnetic Recoil Spectrometer (MRSt) for time-resolved measurements of the neutron spectrum at the National Ignition Facility (NIF),” *Rev. Sci. Instrum.* (these proceedings).
- ¹¹T. J. Hilsabeck *et al.*, “A stretch/compress scheme for a high temporal resolution detector for the Magnetic Recoil Spectrometer time (MRSt),” *Rev. Sci. Instrum.* (these proceedings).
- ¹²I. R. McDonald, A. M. Lamki, and C. F. G. Delaney, *J. Phys. D* **6**, 87 (1973).
- ¹³J. Llacer and E. L. Garwin, *J. Appl. Phys.* **40**, 2766–2775 (1969).
- ¹⁴B. L. Henke *et al.*, *J. Appl. Phys.* **52**, 1509 (1981).
- ¹⁵A. G. Kravchenko *et al.*, *Instrum. Exp. Tech.* **47**, 157 (2004).
- ¹⁶H. Khater and S. Brereton, in *Joint International Conference on Supercomputing Nuclear Applications, Monte Carlo* (LLNL, Tokyo, 2010).
- ¹⁷S. S. Medley and R. Persing, *Rev. Sci. Instrum.* **52**, 1463 (1981).
- ¹⁸J. G. Timothy and R. L. Bybee, *Rev. Sci. Instrum.* **50**, 743 (1979).
- ¹⁹O. L. Landen, *Rev. Sci. Instrum.* **72**, 709 (2001).
- ²⁰N. Sinenian, *Rev. Sci. Instrum.* **83**, 043502 (2012).